BioSystems 262 (2026) 105738

Contents lists available at ScienceDirect

BioSystems

journal homepage: www.elsevier.com/locate/biosystems

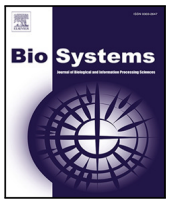

Full Length Article

Clock rate and controllable volume: Physical constraints on biological pacemakers without assuming metabolic scaling

Tatsuaki Tsuruyama[1]

Department of Drug Discovery Medicine, Graduate School of Medicine, Kyoto University, Kyoto 606-8501, Japan
Department of Clinical Laboratory Medicine, Graduate School of Health Science, Kyoto Tachibana University, Kyoto 607-8175, Japan

ARTICLE INFO

Keywords:
Allometry
Scaling law
Heart rate
Pacemaker
Vascular network
Fractal dimension
Information and control
Biological clock

ABSTRACT

How the resting heart rate of mammals scales with body size is a classic allometric problem. Let M denote body mass, V_h heart volume, τ the mean interval period, and $f_H = 1/\tau$. Although quarter-power scaling has been widely cited, reported exponents vary across taxa and physiological states. Here, we derive a constraint-based feasible envelope for resting heart-rate scaling without presupposing any metabolic scaling law; neuroendocrine control and metabolic demand are treated as selecting operating points within this envelope.

We model the heart as a finite three-dimensional pacemaker volume embedded in delayed feedback and limited by sustainable mean power. This yields two generic *lower bounds* on the interbeat period, equivalently *upper bounds* on attainable heart rate: i) a geometric/control bound that grows with the linear size of the heart due to finite propagation/coherence and delay-limited stable control, and ii) a throughput power bound set by the ratio of per-beat energetic cost to maximum sustainable power. Together, these constraints confine feasible heart-rate scaling to an exponent range consistent with observed variability and imply that quarter-power behavior is best viewed as a local effective slope rather than a universal law.

To connect throughput to structure, we use a heuristic mapping between sustainable power and an effective dimension of the vascular network, motivated by the reported 3D microvascular fractal dimensions $D \approx 2.0$–2.6, which correspond to $2/3 \lesssim \gamma \lesssim 0.87$. Importantly, $\gamma \approx 0.75$, often used as a canonical benchmark, is contained in this interval. Re-analysis of a compiled mammalian resting dataset gives an overall heart-rate exponent -0.159, and information criteria favor a single power law. A functional proxy based on maximal oxygen uptake implies a throughput exponent near 0.87, corresponding to an effective dimension near 2.6. Finally, we show that the crossover between geometric/control and power limitation depends on prefactors that cannot be identified from resting heart-rate versus mass data alone, motivating joint datasets combining heart size, ECG timing, e.g., RR/PR/QRS/QT intervals, and cardiac work or power.

1. Introduction

Many physiological traits, including physiological, morphological, biochemical, behavioral, and ecological traits, vary systematically with body size across species, a field known as allometry. Allometric analysis asks how a biological variable changes with body mass M.

In mammals, basal (resting) metabolic rate B scales sublinearly (i.e., with log–log slope $\beta < 1$) with body mass,

$$B \propto M^{\beta}. \tag{1}$$

and its exponent β often reported to be close to 3/4, a well-known empirical regularity referred to as Kleiber's law. A long-standing reason that metabolic scaling and heart-rate scaling are frequently discussed together is the idea that metabolic *demand* (oxygen consumption) and circulatory *supply* (oxygen delivery) should remain broadly matched across size. A representative circulatory variable is cardiac output Q. By Fick's principle,

$$\dot{V}O_2 = Q\,(C_{aO_2} - C_{vO_2}), \tag{2}$$

where $(C_{aO_2} - C_{vO_2})$ is the arteriovenous oxygen content difference (arterial oxygen content C_{aO_2} minus venous oxygen content C_{vO_2}), and Q is cardiac output (Klabunde, 2011). If (as an approximation) oxygen extraction $(C_{aO_2} - C_{vO_2})$ is approximately size-invariant over the relevant range, then $B \propto \dot{V}O_2 \propto Q$ follows. On the other hand, cardiac output is given by heart rate f_H and stroke volume SV as

$$Q = f_H \times SV. \tag{3}$$

E-mail address: tsuruyam@kuhp.kyoto-u.ac.jp.
[1] M.D., Ph.D.

https://doi.org/10.1016/j.biosystems.2026.105738
Received 23 December 2025; Received in revised form 20 February 2026; Accepted 20 February 2026
Available online 26 February 2026

If metabolic rate scales as $B \propto M^{\beta}$ and, as an approximation, stroke volume scales as $SV \propto M^{\delta}$ (with δ treated explicitly because it can vary with taxon, physiological state, and loading conditions), then a simple accounting identity yields

$$f_H \propto \frac{B}{SV} \propto M^{\beta-\delta} \quad \Rightarrow \quad b = \beta - \delta, \tag{4}$$

where b denotes the heart-rate exponent. In many comparative-physiological contexts, especially in interspecific mammalian datasets, δ is often taken to be near unity as an *empirical* approximation (i.e., SV is roughly proportional to body mass over the studied range). We emphasize, however, that this is not a universal geometric consequence: SV is a functional volume difference (end-diastolic minus end-systolic volume) and can depend on ventricular morphology, filling, contractility, and regulation. Under the commonly used $\beta \simeq 3/4$ (Kleiber's law) together with the approximate $\delta \simeq 1$, one obtains the frequently cited consistency relation $b \simeq -1/4$, consistent with classical reports of quarter-power heart-rate scaling (Stahl, 1967; Savage et al., 2004; Bassil et al., 2017; He et al., 2023; Agutter and Wheatley, 2004; Günther and Morgado, 2005). This relation is routinely exploited in the "heart rate method", where heart rate is used as an empirical proxy for oxygen consumption associated with activity, feeding, and digestion (Armstrong, 1986; Esposito et al., 2004; Green et al., 2005; Green, 2011).

Importantly, however, neither the approximate $3/4$ metabolic scaling nor the $-1/4$ heart-rate scaling should be treated as a standalone universal law without specifying taxon, physiological state, environment, and measurement conditions. Indeed, both exponents have been emphasized to vary across contexts (Agutter and Wheatley, 2004; Glazier, 2022).

1.1. Heart rate is a controlled variable: where set-point theory is needed

Heart rate is a *controlled variable* that is actively regulated in response to metabolic demand and behavioral state, rather than a mere geometric consequence of organ size. This regulation is mediated primarily by the autonomic nervous system (sympathetic and parasympathetic branches): the firing frequency of the sinoatrial node increases with greater sympathetic activity (and circulating catecholamines) and decreases with greater vagal activity. Moreover, through feedback to blood pressure, blood gases, and body temperature (e.g., via the baroreflex), interbeat intervals are continuously reset on time scales of seconds to minutes.

In fact, heart rate rises rapidly during exercise or activity (Hedrick et al., 2015; Bishop and Spivey, 2013), and in some lineages covaries strongly with breathing frequency (e.g., respiratory sinus arrhythmia, RSA) (Blawas et al., 2021). In ectotherms, temperature effects are pronounced, and heart rate can change substantially with ambient temperature even within the same individual (Edney, 1964; DeFur and Mangum, 1979). Heart rate has also been widely used as an empirical proxy for oxygen consumption (metabolic rate), while its scope and limitations have been organized and discussed (Green, 2011; Green et al., 2005; Esposito et al., 2004; Armstrong, 1986). Therefore, predicting the observed heart-rate *operating point* (set point) uniquely requires an explicit set-point theory that incorporates neuroendocrine control, behavioral state, metabolic demand, and external conditions such as temperature.

1.2. Relation to existing theory: WBE (West–Brown–Enquist) and the position of this study

A prominent theoretical framework for explaining quarter-power scaling in metabolic rate and heart rate is the West–Brown–Enquist (WBE) model (West et al., 1997, 1999). WBE suggests that when a branching network responsible for resource supply throughout the body follows design principles such as (i) space filling, (ii) approximately size-invariant terminal units (e.g., capillaries), and (iii) some form of transport-cost optimization, metabolic rate B may approach $B \propto M^{3/4}$, and related time scales may exhibit dependencies close to $M^{1/4}$ (West et al., 1997, 1999). The present study aims to connect such metabolic/network theories with physical constraints by separating *metabolic demand and neuroendocrine control* (which can set operating points) from *physical feasibility constraints* (which define the attainable envelope). In this division of labor, metabolic and network theories (including WBE) can inform which operating points are favored within the envelope, while our framework constrains where the envelope lies in the first place, based on finite propagation/coherence, delay-limited stable control, and sustainable mean power throughput. Under this viewpoint, quarter-power scaling is repositioned as a *local effective exponent within the feasible envelope*, consistent with empirical reports that exponents shift with conditions, taxa, and physiological state (Clark and Farrell, 2011; Glazier, 2022).

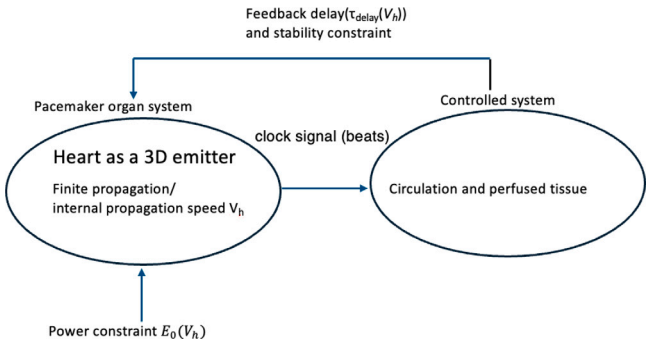

Fig. 1. The heart as a three-dimensional volume-pulse emitter. Propagation/coherence, feedback delay, and sustainable power constrain feasible clock rates; metabolism and control select operating points within the envelope.

2. Results

2.1. Conceptual framework: the heart as a three-dimensional emitter and a one-dimensional clock

We model cardiac *pacemaking* as a finite physical system: a three-dimensional volume V_h that contains supply/dissipation networks (coronary circulation and microvasculature) and generates a contraction sequence that functions as a one-dimensional clock signal for the whole body (Fig. 1).

From this viewpoint, the heart is a three-dimensional emitter that must coordinate a three-dimensional controlled volume (the circulatory system and perfused tissues) via a one-dimensional time code (a beat sequence). In doing so, three generic constraints apply:

1. **Finite internal propagation/coherence speed.** Electrical and mechanical signals do not propagate instantaneously; the larger the heart, the longer excitation propagation and coherent contraction require.
2. **Feedback delay and stability.** The heart is embedded in delayed feedback loops such as baroreflexes, chemoreflexes, and autonomic regulation; stable control requires bandwidth limitation and phase margin.
3. **Finite sustainable mean power.** Each beat consumes energy; the long-time average power required must not exceed the power that can be supplied and dissipated through vascular networks and metabolism.

Consider a pacemaker system parameterized by heart volume V_h. Assuming similarity, a characteristic length L scales as

$$L = c_L V_h^{1/3}, \tag{5}$$

where c_L is a dimensionless geometric constant. The heart generates time-varying flow $Q(t)$ and pressure $p(t)$. For downstream controlled volumes, the essential output is the sequence of beat times $\{t_n\}$ and corresponding stroke volumes $\{\Delta V_n\}$. We therefore abstract cardiac output S as a one-dimensional sequence:

$$S = \{(\tau_n, \Delta V_n)\}_{n=1}^{\infty}, \qquad \tau_n = t_{n+1} - t_n, \tag{6}$$

and define the mean period $\tau = \langle \tau_n \rangle$ and heart rate

$$f_H = \frac{1}{\tau}. \tag{7}$$

Our question is: for a heart of increasing volume V_h, what heart rates $f_H(V_h)$ are feasible while satisfying the above physical constraints?

2.2. Energy scaling and the power constraint

We connect fractal analyses of microvascular and coronary vascular networks to this framework (Table 2). The classical 1/4 rule can appear as one example within a band determined by organ geometry, finite propagation/delay, and the effective dimension of internal vascular networks (Craciunescu et al., 1999; Risser et al., 2007; Cassot et al., 2006; Lorthois and Cassot, 2010; van Bavel and Spaan, 1992).

As a first approximation, we assume that per-beat energy $E_0(V_h)$ is proportional to myocardial volume. If stress–strain–shortening dynamics at the tissue level are size-invariant, then the beat work per unit volume is approximately constant. Thus,

$$E_0(V_h) = k_E V_h, \tag{8}$$

where the proportional coefficient $k_E > 0$ is an effective energy density (J/volume). Beat-wise myocardial energetics has long been linked to mechanical indices such as pressure–volume area (PVA), which correlates with myocardial oxygen consumption per beat; this supports treating per-beat energetic cost as an organ-level quantity that scales with myocardial size under broadly similar loading and contractile regimes (Suga et al., 1980).

Generalization: the exponent η for per-beat energy. If pressure load, wall stress, geometry, or contraction mode change systematically with size, then E_0 may not be strictly proportional to V_h. To make sensitivity explicit, we introduce

$$E_0(V_h) = k_E V_h^{\eta}, \qquad (\eta = 1 \text{ is the baseline of this study}), \tag{9}$$

where η is an effective exponent. The derivations below retain η explicitly and return to $\eta = 1$ when baseline results are discussed. Let $P_{\max}(V_h)$ denote the maximum sustainable mean power that can be allocated to maintaining beating (within survivable bounds that avoid depletion of metabolic supply or overheating). Using a coefficient k_P, we assume

$$P_{\max}(V_h) = k_P V_h^{\gamma}, \tag{10}$$

where γ is a throughput exponent reflecting supply and dissipation constraints.

The mean power required to beat with period τ is

$$P_{\text{beat}}(V_h, \tau) = \frac{E_0(V_h)}{\tau} = \frac{k_E V_h^{\eta}}{\tau}. \tag{11}$$

Viability requires

$$P_{\text{beat}}(V_h, \tau) \le P_{\max}(V_h). \tag{12}$$

Substituting Eqs. (9) and (11) into Eq. (12) yields

$$\frac{k_E V_h^{\eta}}{\tau} \le k_P V_h^{\gamma} \quad \Rightarrow \quad \tau \ge \frac{k_E}{k_P} V_h^{\eta-\gamma}. \tag{13}$$

Here, define the power prefactor

$$c_{\text{pow}} := \frac{k_E}{k_P}. \tag{14}$$

Then the power constraint can be written as

$$\tau_{\text{pow}}(V_h) := c_{\text{pow}} V_h^{\eta-\gamma}, \qquad \tau(V_h) \ge \tau_{\text{pow}}(V_h). \tag{15}$$

In the power-limited regime, heart-rate scaling becomes

$$f_{\text{pow}}(V_h) := \frac{1}{\tau_{\text{pow}}(V_h)} \propto V_h^{\gamma-\eta}. \tag{16}$$

Thus, the exponent relating heart rate to heart volume is

$$f_H \propto V_h^{b_V}, \qquad b_V := \gamma - \eta. \tag{17}$$

Setting $\eta = 1$ recovers the baseline forms used in this study:

$$P_{\text{beat}} = k_E V_h/\tau, \qquad \tau_{\text{pow}} \propto V_h^{1-\gamma}, \qquad f_{\text{pow}} \propto V_h^{\gamma-1}.$$

To connect to body-mass scaling $f_H \propto M^b$, we use the allometry between heart volume and body mass,

$$V_h \propto M^{\alpha}, \tag{18}$$

where α is typically close to unity for mammals at the interspecific scale, but need not be exactly 1.

From Eqs. (16) and (18),

$$f_H \propto V_h^{\gamma-\eta} \propto M^{\alpha(\gamma-\eta)}. \tag{19}$$

Hence,

$$b = \alpha b_V \approx \gamma - \eta \quad (\alpha \simeq 1 \text{ for mammals}). \tag{20}$$

In particular, for the baseline case $\eta = 1$ we obtain

$$b = \alpha(\gamma - 1), \tag{21}$$

which makes explicit how deviations from $\alpha \simeq 1$ or from $\eta = 1$ propagate to the observed heart-rate exponent b.

3. Constraints from propagation and control

3.1. Internal propagation/coherence (a hard feasibility constraint)

Within the heart, electrical excitation and mechanical waves propagate through the tissue and conduction pathways at finite speeds. Let c_{eff} denote an *effective coherence speed* that includes electrical conduction, mechanical synchronization, and electromechanical coupling.

The time required for a coherence signal to traverse the organ is at least, for a transverse distance L,

$$\tau_{\text{prop}}(V_h) := \frac{L}{c_{\text{eff}}} = \frac{c_L}{c_{\text{eff}}} V_h^{1/3} =: c_{\text{prop}} V_h^{1/3}, \tag{22}$$

with $c_{\text{prop}} := c_L/c_{\text{eff}}$. If coordinated contraction is to be achieved within each beat, the cardiac period cannot be arbitrarily shorter than this coherence time. Thus,

$$\tau(V_h) \ge \tau_{\text{prop}}(V_h) = c_{\text{prop}} V_h^{1/3}. \tag{23}$$

Violating this bound would lead to loss of coherent activation, and therefore failure of effective pumping. In this sense, Eq. (23) constitutes a *hard feasibility constraint* rather than a soft regulatory influence.

Accordingly, the propagation-limited heart-rate scaling satisfies

$$f_{\text{prop}}(V_h) \lesssim V_h^{-1/3}, \tag{24}$$

which arises purely from three-dimensional geometry combined with finite propagation/coherence speed.

Quantitative note (clarifying interpretation). In humans, ventricular activation occurs on a time scale much shorter than the interbeat interval at rest (Klabunde, 2011). For example, activation/coordination times are on the order of $\lesssim$0.1 s, whereas resting beat periods are typically ~0.6–1 s; Purkinje conduction velocities are on the order of meters per second (Klabunde, 2011). This implies that under normal physiology, conduction time is not a *proximal control factor* determining the resting operating point. Thus, Eq. (23) is used as a *hard feasibility bound* on attainable rates with increasing size, not as a claim that conduction time sets the set point. Further related discussion and implications are provided in the Discussion section.

3.2. Feedback delay and phase margin

The heart is embedded in feedback loops involving autonomic and hormonal pathways that regulate blood pressure, cardiac output, and metabolic variables. Let $\tau_{\mathrm{delay}}(V_h)$ denote the effective feedback delay relevant to heart-rate control.

In a feedback loop with crossover frequency ω_c, the phase margin decreases approximately by $\omega_c \tau_{\mathrm{delay}}$. As a conservative stability requirement, we impose

$$\omega_c \tau_{\mathrm{delay}}(V_h) \lesssim \Phi_m, \tag{25}$$

where Φ_m is the target phase margin required for stable regulation.

Assuming that the crossover frequency is on the order of the heart-rate angular frequency, $\omega_c \sim 2\pi f$, we obtain

$$2\pi f\, \tau_{\mathrm{delay}}(V_h) \lesssim \Phi_m \quad \Rightarrow \quad f \lesssim c_{\mathrm{pm}} \frac{1}{\tau_{\mathrm{delay}}(V_h)}, \tag{26}$$

with $c_{\mathrm{pm}} := \Phi_m/(2\pi)$. Equivalently,

$$\tau(V_h) \gtrsim c_{\mathrm{pm}}\, \tau_{\mathrm{delay}}(V_h). \tag{27}$$

Because signal pathways (neural and hemodynamic) lengthen with increasing heart and body size, we expect $\tau_{\mathrm{delay}}(V_h)$ to increase with size. For simplicity, we assume that the dominant contribution scales with the same characteristic length L:

$$\tau_{\mathrm{delay}}(V_h) = c_{\mathrm{delay}} V_h^{1/3}. \tag{28}$$

Then the stability-derived lower bound on the period becomes

$$\tau_{\mathrm{stab}}(V_h) := c_{\mathrm{pm}} c_{\mathrm{delay}} V_h^{1/3} =: c_{\mathrm{stab}} V_h^{1/3}, \tag{29}$$

and therefore

$$\tau(V_h) \geq \tau_{\mathrm{stab}}(V_h). \tag{30}$$

3.3. Unified geometric/control constraint

Combining the propagation and feedback-delay constraints, we define a unified geometric/control lower bound on the cardiac period:

$$\tau_{\mathrm{geom}}(V_h) := c_{\mathrm{geom}} V_h^{1/3}, \tag{31}$$

where

$$c_{\mathrm{geom}} := \max(c_{\mathrm{prop}}, c_{\mathrm{stab}}). \tag{32}$$

Thus, the unified geometric/control feasibility condition is

$$\tau(V_h) \geq \tau_{\mathrm{geom}}(V_h) = c_{\mathrm{geom}} V_h^{1/3}. \tag{33}$$

The corresponding heart-rate scaling implied by this bound is

$$f_{\mathrm{geom}}(V_h) \lesssim V_h^{-1/3}. \tag{34}$$

4. Overall lower bound on the cardiac period and regime structure

The cardiac period τ must satisfy both the geometric/control constraint (Eq. (33)) and the power constraint (Eq. (13)). Therefore,

$$\tau(V_h) \geq \max\left\{\tau_{\mathrm{geom}}(V_h),\, \tau_{\mathrm{pow}}(V_h)\right\} = \max\left\{c_{\mathrm{geom}} V_h^{1/3},\, c_{\mathrm{pow}} V_h^{\eta-\gamma}\right\}. \tag{35}$$

Focusing on scaling exponents only and adopting the baseline case $\eta = 1$, we may write

$$\tau(V_h) \sim V_h^{\zeta_*}, \qquad \zeta_* := \max\left(\frac{1}{3},\, 1-\gamma\right), \tag{36}$$

where ζ_* denotes the effective scaling exponent of the minimal feasible period.

Accordingly, the feasible heart-rate scaling becomes

$$f_H(V_h) \sim V_h^{-\zeta_*}. \tag{37}$$

4.1. Range of γ: constraints from supply and dissipation in three-dimensional tissue

We now constrain the throughput exponent γ from general considerations of supply and dissipation in three-dimensional organs.

If the maximum sustainable mean power is determined by the number of active units (e.g., cardiomyocytes), and if the contribution of each unit is approximately size-invariant, then

$$P_{\mathrm{max}} \propto N_{\mathrm{active}} \propto V_h, \tag{38}$$

corresponding to $\gamma = 1$. In a healthy heart with broadly similar cellular properties across species, it is unlikely that P_{max} increases faster than volume, so we expect

$$\gamma \leq 1. \tag{39}$$

On the other hand, if sustainable power is limited by surface-mediated processes such as oxygen or nutrient delivery, or by heat dissipation, then for a compact organ

$$A \propto r^2 \propto V_h^{2/3}, \tag{40}$$

and therefore

$$P_{\mathrm{max}} \propto A \propto V_h^{2/3}, \tag{41}$$

corresponding to $\gamma = 2/3$. Values $\gamma < 2/3$ would imply that P_{max} grows more slowly than surface area, leading to an extreme power deficit for large hearts, which is physiologically implausible. We therefore adopt

$$\frac{2}{3} \lesssim \gamma \lesssim 1 \tag{42}$$

as a physically reasonable range.

4.2. Consequence for heart-rate scaling: the exponent envelope

From Eq. (42), the power-constraint exponent $1-\gamma$ lies in

$$1-\gamma \in \left[0,\, \frac{1}{3}\right]. \tag{43}$$

Comparing this range with the geometric/control exponent $1/3$ in Eq. (36), we find that for sufficiently large V_h the geometric/control constraint

$$\tau \propto V_h^{1/3} \tag{44}$$

becomes asymptotically dominant, yielding

$$f_H(V_h) \sim V_h^{-1/3}. \tag{45}$$

Over intermediate size ranges, however, the power constraint may dominate, in which case

$$f_H(V_h) \sim V_h^{\gamma-1}. \tag{46}$$

For the baseline case $\eta = 1$, the feasible heart-rate exponents (with respect to V_h) are confined to

$$-\frac{1}{3} \leq b_V \leq 0. \tag{47}$$

The classical quarter-power exponent $-1/4$ corresponds to

$$\gamma = \frac{3}{4}, \tag{48}$$

which lies naturally within this envelope.

4.3. Crossover between geometric/control and power constraints

We refer to the boundary at which the dominant lower bound on the cardiac period switches between the geometric/control constraint and the power constraint as the *crossover*.

The crossover volume V_h^* is defined implicitly by the condition

$$\tau_{\mathrm{geom}}(V_h^*) = \tau_{\mathrm{pow}}(V_h^*). \tag{49}$$

Using Eq. (35), this yields

$$c_{\mathrm{geom}} V_h^{1/3} \sim c_{\mathrm{pow}} V_h^{1-\gamma} \quad \Rightarrow \quad V_h^* \sim \left(\frac{c_{\mathrm{pow}}}{c_{\mathrm{geom}}} \right)^{\frac{1}{\gamma - 2/3}}. \tag{50}$$

Because the exponent $(\gamma - 2/3)^{-1}$ diverges as $\gamma \to 2/3$, even modest uncertainty in the prefactor ratio $c_{\mathrm{pow}}/c_{\mathrm{geom}}$ can shift the crossover volume by orders of magnitude. This sensitivity underlies the empirical difficulty of locating the crossover from resting heart-rate data alone.

5. Network dimension and vascular fractal structure

So far, the throughput exponent γ has been constrained only by inequalities. To connect scaling more directly to internal anatomy, we now introduce the effective dimension D_{eff} of the supply/dissipation vascular network.

5.1. Effective network dimension D_{eff}

Consider the coronary circulation and microvascular networks that supply oxygen and nutrients to the myocardium and remove heat and metabolic waste. These networks are embedded in three-dimensional space, are highly branched, and exhibit multiscale self-similarity. Fractal analyses of vascular trees and microvasculature often report non-integer dimensions between 2 and 3 for three-dimensional data (Craciunescu et al., 1999; Risser et al., 2007; Cassot et al., 2006; Lorthois and Cassot, 2010) (Table 2). The branching morphology of mammalian coronary arteries has also been quantified (e.g., porcine coronary trees) (van Bavel and Spaan, 1992).

If the vascular network effectively fills a subset of dimension D_{eff}, then the maximum sustainable throughput per unit time may scale as

$$P_{\max}(V_h) \propto V_h^{D_{\mathrm{eff}}/3}. \tag{51}$$

Comparing Eqs. (10) and (51) yields the correspondence

$$\gamma = \frac{D_{\mathrm{eff}}}{3}. \tag{52}$$

Combining this with the power-limited heart-rate scaling $f_H \propto V_h^{\gamma-1}$ and the heart–body allometry $V_h \propto M^{\alpha}$ gives

$$f_H \propto M^{\alpha(\gamma-1)} = M^{\alpha(D_{\mathrm{eff}}/3-1)}. \tag{53}$$

Thus, the heart-rate exponent can be written as

$$b = \alpha \left(\frac{D_{\mathrm{eff}}}{3} - 1 \right). \tag{54}$$

If heart volume scales approximately linearly with body mass ($\alpha \simeq 1$), as is typical for mammals at the interspecific scale, then

$$b \approx \frac{D_{\mathrm{eff}} - 3}{3}. \tag{55}$$

Eq. (51) should be viewed as a *heuristic throughput ansatz*. Fluid resistance, heterogeneity, safety margins, and deviations from strict fractality can modify the mapping between D_{eff} and $P_{\max}$. The framework is therefore explicitly falsifiable: independent measurements of cardiac (or coronary/microvascular) structure and heart-rate allometry in the same species set can directly test the proposed correspondence.

Even if vascular structure exhibits an effective dimension D_{eff}, maximum sustainable throughput may be limited by additional mechanisms such as flow resistance (e.g., pressure losses and viscous dissipation), perfusion heterogeneity and shunting, safety margins against ischemia, and non-similar changes in coronary reserve. These effects can alter the mapping between D_{eff} and $P_{\max}$ without invalidating the envelope logic, and can be absorbed into an effective exponent γ and prefactor k_P in Eq. (10). This motivates direct, heart-specific measurements of structural proxies and performance limits in matched species sets as decisive tests.

Table 1
Model comparison among single power law, piecewise regression, and smooth transition using AIC/BIC (smaller is better). Both criteria favor the single power law, providing no evidence that a breakpoint is required for this compilation.

Model	k	SSE	AIC	BIC
Single power (single)	2	0.889	−80.40	−75.30
Piecewise (continuous)	4	0.845	−77.60	−67.38
Smooth transition (soft-hinge)	5	0.838	−75.60	−62.83

5.2. Empirical values of D_{eff} and implications

Three-dimensional analyses of microvascular networks in the brain, skeletal muscle, tumors, and other tissues report fractal dimensions $D \approx 2.0$–2.6 (Craciunescu et al., 1999; Risser et al., 2007; Cassot et al., 2006; Lorthois and Cassot, 2010). For example, Craciunescu et al. reported $D \approx 2.0$–2.3 in normal tissue casts and up to ≈ 2.6 in tumor vasculature (Craciunescu et al., 1999). Risser et al. and Cassot et al. reported region- and layer-dependent values $D \approx 2.0$–2.5 (Risser et al., 2007; Cassot et al., 2006). Morphogenetic models of vascular formation also reproduce realistic networks with $D \approx 2.3$–2.8 (Lorthois and Cassot, 2010).

Taken together, a representative range is

$$2.0 \lesssim D_{\mathrm{eff}} \lesssim 2.6. \tag{56}$$

Substituting into Eq. (52) gives

$$\gamma = \frac{D_{\mathrm{eff}}}{3} \in [0.67,\ 0.87], \tag{57}$$

and thus

$$b_V = \gamma - 1 \in [-0.33,\ -0.13], \tag{58}$$

which is consistent with reported mammalian heart-rate exponents.

Extrapolation from tissue to heart (reviewer clarification). Because systematic three-dimensional surveys of *cardiac* microvasculature across matched species are limited, Table 2 includes values from diverse tissues. These serve as plausible priors motivating the D_{eff}–b correspondence and a concrete, testable prediction: measure D_{eff} (or close proxies of coronary/microvascular structure) in the heart for the same species set and compare directly with heart-rate allometry.

6. Empirical re-analysis and context dependence

6.1. Data and preprocessing

We used the mammalian resting heart-rate compilation of Travasso et al. (2025). Analyses were performed after log–log transformation with $x = \log_{10} M$ and $y = \log_{10} f_H$. We compared three models:

1. **Single power law**:
$$y = \log_{10} a + b\, x. \tag{59}$$
2. **Piecewise linear (continuous join)**:
$$y = a + b_1 x + (b_2 - b_1) \max(0,\ x - x^*), \tag{60}$$
with continuity at x^*.
3. **Smooth transition (soft-hinge)**: a continuous transition obtained by smoothing $\max(0, \cdot)$ (e.g., softplus).

6.2. Estimation and information criteria (AIC/BIC)

Each model was estimated by least squares and compared using Akaike Information Criterion (AIC) and Bayesian Information Criterion (BIC) under approximate normal residuals. The single power-law

Table 2
Representative 3D fractal dimensions reported for microvascular networks and related models (candidate effective network dimensions D_{eff}).

Study	Tissue/Species	Method	Reported fractal dimension
Craciunescu et al. (1999)	Normal vs. tumor tissue	3D box-counting	$D \approx 2.0$–2.6
Risser et al. (2007)	Brain microvasculature	SR-CT	$D \approx 2.3$–2.7
Cassot et al. (2006)	Human cerebral cortex	3D reconstruction	$D \approx 2.0$–2.5
Lorthois and Cassot (2010)	Morphogenetic model	Growth model	$D \approx 2.3$–2.8

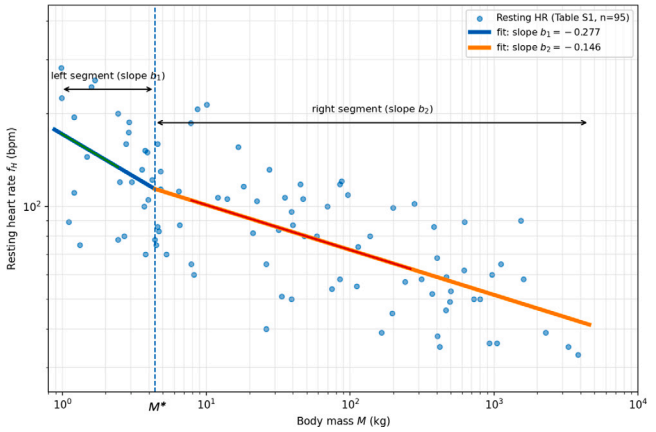

Fig. 2. Log–log relationship between resting mammalian heart rate and body mass. Single power-law fit versus transition models. AIC/BIC favor a single power law. The symbol M^* denotes the nominal breakpoint returned by a continuous piecewise fit, but its location is uncertain and a breakpoint is not required by model selection.

model has $k = 2$ parameters, the continuous piecewise model has $k = 4$, and the smooth transition model has $k = 5$. The Ordinary Least Squares(OLS) fit for the single power law yielded $b \simeq -0.159$, corresponding to $f_H \propto M^{-0.16}$. Allowing a continuous breakpoint can reduce SSE slightly (e.g., piecewise regression yields slopes such as $b_1 \simeq -0.277$ and $b_2 \simeq -0.146$ with a nominal breakpoint near $M^* \simeq 4\,\mathrm{kg}$), but the breakpoint location is uncertain and the added flexibility is not supported by information criteria.

Importantly, both AIC and BIC favor the single power law (Table 1). Thus, there is no statistical evidence that a breakpoint is required in this compilation; the simpler OLS model is sufficient at the dataset level, consistent with the scatter in Fig. 2. We therefore treat the piecewise and smooth-transition fits as exploratory comparisons that illustrate how local effective slopes (including values near $-1/4$ over restricted mass ranges) can arise without implying a discrete anatomical transition.

From Table 1, the single power law is preferred under both AIC and BIC. Although more complex models reduce SSE, the improvement does not justify additional parameters. However, continuous piecewise fits can yield local slope candidates near $-1/4$ (small bodies) and near -0.1 (large bodies), consistent with context dependence rather than a required breakpoint.

A functional (non-fractal) proxy estimate of γ from maximal oxygen uptake. To estimate throughput without invoking fractal geometry, we use maximal oxygen uptake as a functional proxy:

$$P_{\max} \propto \dot{V}O_{2,\max}. \tag{61}$$

Because the oxycaloric conversion changes only a prefactor, not the log–log slope, we define

$$\gamma := \frac{d \log P_{\max}}{d \log V_h} \approx \frac{d \log \dot{V}O_{2,\max}}{d \log V_h}, \qquad D_{\mathrm{eff}} := 3\gamma. \tag{62}$$

This is consistent with Fick's principle,

$$\dot{V}O_{2,\max} = CO_{\max}\, \Delta C_{\mathrm{O}_2,\max}. \tag{63}$$

If $\dot{V}O_{2,\max} \propto M^{\beta}$ and $V_h \propto M^{\alpha}$ (allowing $\Delta C_{\mathrm{O}_2,\max} \propto M^{\epsilon}$), then

$$\gamma \approx \frac{\beta - \epsilon}{\alpha}. \tag{64}$$

A synthesis of mammalian maximal exercise metabolism reports $\beta \simeq 0.87$ (Weibel et al., 2004; Weibel and Hoppeler, 2005). With near-isometric heart scaling $\alpha \simeq 1$, this yields

$$\gamma \simeq 0.87, \qquad D_{\mathrm{eff}} \simeq 2.6, \tag{65}$$

consistent with the plausible D_{eff} range in Table 2.

Discussion

Applicability: feasibility bounds versus physiological set points

The present theory is not intended to predict resting heart-rate set points from first principles. Rather, it provides physically motivated *feasibility bounds* on attainable cardiac clock rates as size increases, derived from propagation/coherence, delay-limited stability, and sustainable power throughput. Neuroendocrine regulation and metabolic demand are then interpreted as selecting state-dependent operating points *within* these bounds (rest, exercise, temperature, ontogeny), consistent with decades of physiological evidence. In addition, ontogenetic trajectories can exhibit systematic shifts in heart rate and its scaling, reflecting developmental changes in morphology and regulation; thus, ontogeny should be treated explicitly when comparing allometric exponents across studies (Spicer and Morritt, 1996).

Separating set points and feasibility (the envelope)

Heart rate is a controlled variable regulated by neuroendocrine feedback and state. Rather than predicting resting set points, this study derives a *feasible envelope* from physical constraints — finite propagation/coherence, delay-limited stable control, and sustainable mean power throughput — that bounds attainable clock rates as size changes. Within this framing, metabolic demand and autonomic/endocrine regulation act as *selectors* of operating points inside the feasible region, while the physical constraints delimit the region itself.

Repositioning quarter-power

The classical $-1/4$ emerges here as a local effective exponent within the envelope $[-1/3, 0]$, not as a universal law. In our framework, quarter-power behavior corresponds to a throughput exponent $\gamma \simeq 3/4$ (baseline $\eta = 1$) within the power-limited regime, but the observed slope can shift with state (rest vs. exercise), taxon, ecology,

measurement conditions, and control strategy. Local slopes near $-1/4$ can therefore coexist with global fits favoring a single power law when geometric/control bounds progressively flatten scaling at large sizes or when datasets mix conditions and groups.

Possible sources of an apparent slope change above M^*. Although information criteria favor a single power law in the present compilation, segmented fits can return an apparent breakpoint near $M^* \sim 4\,\mathrm{kg}$. We emphasize that such a breakpoint need not imply a sharp anatomical transition. First, cardiac electrical time scales (RR, PR, QRS, QT) exhibit systematic allometry across mammals, consistent with size-dependent changes in conduction pathway lengths and electrophysiological timing (Günther and Morgado, 1997; Storlund et al., 2021). Second, size-dependent shifts in ventricular geometry, loading, and coronary reserve can primarily alter prefactors (and potentially weakly affect the effective per-beat cost exponent), which can move the apparent crossover in finite datasets without requiring distinct exponents. Third, compiled datasets may mix clades and measurement conditions (e.g., anesthetized vs. conscious; terrestrial vs. marine), and these grouping factors can correlate with body mass and generate piecewise-looking patterns even when the underlying relationship is continuous (Storlund et al., 2021). More generally, diverse scaling slopes can arise within physical boundary limits under contingent anatomical and physiological influences (Glazier, 2014).

Crossover and identifiability

The crossover between geometric/control limitation and power limitation depends sensitively on prefactors c_{geom} and c_{pow}, not only on exponents. Resting f_H–M compilations alone cannot identify the crossover, reflecting an identifiability limitation rather than a fitting failure. Joint datasets combining ECG timing (as a proxy for conduction/coordination and delay scales), heart size $V_h(M)$, and cardiac work/power (or performance limits) are required to constrain these prefactors. Here, "ECG timing" refers to standard electrocardiographic interval measures such as RR (beat-to-beat period), PR (atrioventricular conduction), QRS (ventricular depolarization/activation), and QT (repolarization) durations; together these provide species-level proxies for excitation/coordination and electromechanical delay scales relevant to c_{geom}. Order-of-magnitude estimates of V_h^* may be possible given species-level proxies for c_{geom} and c_{pow}, but because such matched datasets are presently limited, we refrain from reporting a potentially misleading estimate here.

Quantitative note (interpretation check). A human timing example is given above to clarify that the geometric/control condition is intended as a feasibility bound rather than a determinant of resting set points. To avoid redundancy, we do not repeat the numerical values here. The key interspecific implication is that resting operating points can lie well above the bound; therefore, locating the crossover requires species-matched proxies for the prefactors (e.g., ECG timing for conduction/coordination and delay scales, together with heart size and cardiac work/power), not resting f_H–M compilations alone.

Illustrative order-of-magnitude (human; not generalized across species). To give a concrete scale without over-interpreting cross-species implications, one may form a human-only estimate of the prefactor gap between the geometric/control bound and the resting operating point. Let τ_{act} denote a characteristic activation/coordination time scale (including ventricular activation and electromechanical synchronization), which is on the order of $\tau_{\mathrm{act}} \lesssim 0.1$ s in humans (Klabunde, 2011), whereas the resting interbeat period is $\tau_{\mathrm{rest}} \sim 0.6$–$1$ s. If $\tau_{\mathrm{geom}} \sim c_{\mathrm{geom}} V_h^{1/3}$ is interpreted as a lower hard-finessibility bound with a prefactor set by such coordination scales, then the human ratio $\tau_{\mathrm{rest}}/\tau_{\mathrm{geom}}$ is plausibly $\mathcal{O}(6$–$10)$ at rest. This illustrates that resting humans operate well above the bound, but it does *not* locate the interspecific crossover: estimating V_h^* in Eq. (50) still requires species-matched prefactors (or proxies) for both c_{geom} and c_{pow}, which are not identifiable from resting f_H–M alone.

Sensitivity via η

Generalizing the per-beat energy as $E_0(V_h) \propto V_h^{\eta}$ makes the sensitivity explicit: the power-limited scaling becomes $f_{\mathrm{pow}}(V_h) \propto V_h^{\gamma-\eta}$ and $b = \alpha b_V$. Thus, deviations in η shift the effective exponent linearly while preserving the envelope logic based on competing lower bounds on τ. This formulation clarifies which empirical quantities (energy-per-beat scaling and sustainable throughput scaling) control the predicted slopes.

Future tests

We will assess robustness across datasets and taxonomic subsets by (i) stratified regressions across major clades and ecologies and (ii) re-fitting the single-power model to at least one independent compilation when available, reporting the overlap of confidence intervals for b. Several tests can directly probe the framework. First, perform stratified regressions for terrestrial versus aquatic groups and across major phylogenetic clades to separate group-level differences (intercepts/slopes) from the effects of pure size (He et al., 2023; Blawas et al., 2021). Second, measure cardiac (coronary/microvascular) structural proxies for D_{eff} in a set of matched species and test the proposed correspondence between b and D_{eff}. Third, extend analyses beyond rest to exercise and maximal conditions, where control bandwidth and throughput limits are more proximal to performance and where state-dependent scaling differences are expected. Fourth, assemble joint datasets that include ECG timing, heart size, pressures/flows, and cardiac work/power, enabling empirical constraints on c_{geom} and c_{pow} and a quantitative evaluation of whether real hearts operate near the crossover. The results are demonstrated for resting mammals using a single compilation. Extension to other taxa, temperatures, physiological states (including exercise), and ontogenetic stages is within the conceptual scope of the framework but remains to be tested quantitatively. Comparisons across studies should explicitly account for developmental (ontogenetic) differences (Spicer and Morritt, 1996).

Conclusions

We proposed a constraint-based framework that distinguishes physiological *set points* from physical *feasibility*. By modeling the heart as a finite three-dimensional pacemaking volume embedded in delayed feedback and limited by sustainable mean power, we derived two generic lower bounds on the interbeat period: a geometric/control bound scaling as $\tau_{\mathrm{geom}} \propto V_h^{1/3}$ and a throughput bound $\tau_{\mathrm{pow}} \propto V_h^{\eta-\gamma}$. Their combination yields a feasible exponent envelope for heart-rate scaling and repositions quarter-power behavior as a context-dependent local effective slope rather than a universal law. The mapping between throughput scaling and internal structure via an effective network dimension D_{eff} is heuristic but testable, and the theory highlights a key identifiability limitation: locating crossover requires prefactors not recoverable from resting f_H–M compilations alone. Future joint structural–functional datasets across taxa, states, and development can therefore provide decisive tests of the proposed envelope and its links to anatomy and control.

CRediT authorship contribution statement

Tatsuaki Tsuruyama: Writing – original draft, Methodology, Conceptualization.

Funding

This study received no external funding.

Declaration of competing interest

We confirm that no authors of this manuscript have any competing financial or non-financial interests, currently or previously, including serving in an editorial capacity for the journal we are submitting to.

Data availability

No data was used for the research described in the article.

References

Agutter, P.S., Wheatley, D.N., 2004. Metabolic scaling: consensus or controversy? Theor. Biol. Med. Model. 1, 13. http://dx.doi.org/10.1186/1742-4682-1-13.

Armstrong, J.D., 1986. Heart rate as an indicator of activity, metabolic rate, food intake and digestion in pike, *Esox lucius*. J. Fish Biol. 29, 207–221. http://dx.doi.org/10.1111/j.1095-8649.1986.tb05012.x.

Bassil, Guillaume, Zarzoso, Manuel, Noujaim, Sami F., 2017. Allometric scaling of electrical excitation and propagation in the mammalian heart. J. Theoret. Biol. 419, 238–242. http://dx.doi.org/10.1016/j.jtbi.2016.09.024.

Bishop, C.M., Spivey, R.J., 2013. Integration of exercise response and allometric scaling in endotherms. J. Theoret. Biol. 323, 11–19. http://dx.doi.org/10.1016/j.jtbi.2013.01.002.

Blawas, A.M., Nowacek, D.P., Rocho-Levine, J., Robeck, T.R., Fahlman, A., 2021. Scaling of heart rate with breathing frequency and body mass in cetaceans. Philos. Trans. R. Soc. B 376 (1830), 20200223. http://dx.doi.org/10.1098/rstb.2020.0223.

Cassot, Franck, Lauwers, Fabien, Fouard, Claude, Prohaska, Stephan, Lauwers-Cances, Valérie, 2006. A novel three-dimensional computer-assisted method for a quantitative study of microvascular networks of the human cerebral cortex. Microcirc. 13 (1), 1–18. http://dx.doi.org/10.1080/10739680500383407.

Clark, T.D., Farrell, A.P., 2011. Effects of body mass on physiological and anatomical parameters of mature salmon: evidence against a universal heart rate scaling exponent. J. Exp. Biol. 214 (6), 887–893. http://dx.doi.org/10.1242/jeb.051607.

Craciunescu, Oana, Das, Shiva K., Dewhirst, Mark W., 1999. Three-dimensional microvascular networks fractal structure: potential for tissue characterization? pp. 1–6, Conference/technical paper (PDF, 6 pp.). URL https://pdodds.w3.uvm.edu/files/papers/others/2002/2002disease/claudio_asme99.pdf. (Accessed 15 February 2026).

DeFur, P.L., Mangum, C.P., 1979. The effects of environmental variables on the heart rates of invertebrates. Comp. Biochem. Physiol. A 62 (2), 283–294. http://dx.doi.org/10.1016/0300-9629(79)90058-6.

Edney, E.B., 1964. Acclimation to temperature in terrestrial isopods: II. Heart rate and standard metabolic rate. Physiol. Zoöl. 37 (4), 378–394. http://dx.doi.org/10.1086/physzool.37.4.30152756.

Esposito, F., Impellizzeri, F.M., Margonato, V., Vanni, R., Pizzini, G., Veicsteinas, A., 2004. Validity of heart rate as an indicator of aerobic demand during soccer activities in amateur soccer players. Eur. J. Appl. Physiol. 93 (1), 167–172. http://dx.doi.org/10.1007/s00421-004-1192-4.

Glazier, Douglas S., 2014. Scaling of metabolic scaling within physical limits. Syst. 2 (4), 425–450. http://dx.doi.org/10.3390/systems2040425.

Glazier, D.S., 2022. Variable metabolic scaling breaks the law: from 'Newtonian' to 'Darwinian' approaches. Proc. R. Soc. B 289 (1985), 20221605. http://dx.doi.org/10.1098/rspb.2022.1605.

Green, J.A., 2011. The heart rate method for estimating metabolic rate: review and recommendations. Comp. Biochem. Physiol. A 158 (3), 287–304. http://dx.doi.org/10.1016/j.cbpa.2010.09.011.

Green, J.A., White, C.R., Butler, P.J., 2005. Allometric estimation of metabolic rate from heart rate in penguins. Comp. Biochem. Physiol. A 142 (4), 478–484. http://dx.doi.org/10.1016/j.cbpa.2005.09.019.

Günther, B., Morgado, E., 1997. Allometry of ECG waves in mammals. Biol. Res. 30, 167–170.

Günther, Bruno, Morgado, Enrique, 2005. Allometric scaling of biological rhythms in mammals. Biol. Res. 38 (2–3), 207–212. http://dx.doi.org/10.4067/S0716-97602005000200010.

He, J., et al., 2023. Allometric scaling of metabolic rate and cardiorespiratory variables in aquatic and terrestrial mammals. Physiol. Rep. 11 (11), e15698. http://dx.doi.org/10.14814/phy2.15698.

Hedrick, M.S., Hancock, T.V., Hillman, S.S., 2015. Metabolism at the max: how vertebrate organisms respond to physical activity. Compr. Physiol. 5 (4), 1677–1703. http://dx.doi.org/10.1002/cphy.c130032.

Klabunde, R., 2011. Cardiovascular Physiology Concepts. Lippincott Williams & Wilkins.

Lorthois, Sébastien, Cassot, Franck, 2010. Fractal analysis of vascular networks: insights from morphogenesis. J. Theoret. Biol. 262 (4), 614–633. http://dx.doi.org/10.1016/j.jtbi.2009.10.037.

Risser, L., et al., 2007. From homogeneous to fractal normal and tumorous microvascular networks in the brain. J. Cereb. Blood Flow Metab. 27, 293–303. http://dx.doi.org/10.1038/sj.jcbfm.9600332.

Savage, V.M., et al., 2004. The predominance of quarter-power scaling in biology. Funct. Ecol. 18, 257–282. http://dx.doi.org/10.1111/j.0269-8463.2004.00856.x.

Spicer, J.I., Morritt, D., 1996. Ontogenic changes in cardiac function in crustaceans. Comp. Biochem. Physiol. A 114 (1), 81–89. http://dx.doi.org/10.1016/0300-9629(95)02095-0.

Stahl, W.R., 1967. Scaling of respiratory variables in mammals. J. Appl. Physiol. 22 (3), 453–460. http://dx.doi.org/10.1152/jappl.1967.22.3.453.

Storlund, Rhea L., Rosen, David A.S., Trites, Andrew W., 2021. Electrocardiographic scaling reveals differences in electrocardiogram interval durations between marine and terrestrial mammals. Front. Physiol. 12, 690029. http://dx.doi.org/10.3389/fphys.2021.690029.

Suga, Hiroyuki, Hayashi, Takakazu, Shirahata, Machiko, Ninomiya, Ishio, 1980. Critical evaluation of left ventricular systolic Pressure Volume Area as predictor of oxygen consumption rate. Jpn. J. Physiol. 30 (6), 907–919. http://dx.doi.org/10.2170/jjphysiol.30.907.

Travasso, R.D.M., Penick, C.A., Dunn, R.R., Corvera Poiré, E., 2025. Predicting cardiac frequencies in mammals. Sci. Rep. 15, 7017. http://dx.doi.org/10.1038/s41598-025-90928-x.

van Bavel, E., Spaan, J.A., 1992. Branching patterns in the porcine coronary arterial tree: Estimation of flow heterogeneity. Circ. Res. 71 (5), 1200–1212. http://dx.doi.org/10.1161/01.RES.71.5.1200.

Weibel, E.R., Bacigalupe, L.D., Schmitt, B., Hoppeler, H., 2004. Allometric scaling of maximal metabolic rate in mammals: muscle aerobic capacity as a determinant factor. Respir. Physiol. Neurobiol. 140 (2), 115–132. http://dx.doi.org/10.1016/j.resp.2004.01.006.

Weibel, E.R., Hoppeler, H., 2005. Exercise-induced maximal metabolic rate scales with muscle aerobic capacity. J. Exp. Biol. 208, 1635–1644. http://dx.doi.org/10.1242/jeb.01548.

West, Geoffrey B., Brown, James H., Enquist, Brian J., 1997. A general model for the origin of allometric scaling laws in biology. Sci. 276 (5309), 122–126. http://dx.doi.org/10.1126/science.276.5309.122.

West, Geoffrey B., Brown, James H., Enquist, Brian J., 1999. A general model for the structure and allometry of plant vascular systems. Nature 400, 664–667. http://dx.doi.org/10.1038/23251.